International Journal of Modern Physics B
Vol. 22, Nos. 9, 10 & 11 (2008) 1775–1782
© World Scientific Publishing Company

World Scientific
www.worldscientific.com

DEFORMATION BEHAVIORS OF Zr-BASED BULK METALLIC GLASS UNDER IMPACT INDENTATION

HYUNG-SEOP SHIN*, SOON-NAM CHANG [1] and DO KYUNG KIM [2]

School of Mechanical Engineering, Andong National University
Andong, Kyungbuk, 760-749, Korea
hsshin@andong.ac.kr
[1] *Agent for Defense Development, Yuseong, Daejeon, 305-600 Korea*
snchang33@hanmail.net
[2] *Department of Materials Science and Engineering, KAIST, Daejeon, 305-701 Korea*
dkkim@kaist.ac.kr

Received 31 July 2007
Revised 9 January 2008

Metallic glasses are amorphous meta-stable solids and are now being processed in bulk form suitable for structural applications under impact loading. Bulk metallic glasses have many unique mechanical properties such as high yield strength and fracture toughness, good corrosion and wear resistance that distinguish them from crystalline metals and alloys. However, only a few studies could be found mentioning the dynamic response and damage of metallic glasses under impact or shock loading. In this study, we employed a small explosive detonator for the dynamic indentation to a Zr-based bulk amorphous metal in order to evaluate the damage behavior of bulk amorphous metal under impact or shock loading conditions. Results were compared with those of spherical indentation under quasi-static and impact loading and were discussed. The interface bonded specimen method was adopted in order to observe the subsurface damage, especially the formation of shear bands induced during indentation under different loading conditions.

Keywords: Bulk Metallic Glass; Strain Rate; Shear Bands; Explosive Indentation; Interface Bonded Specimen Method.

1. Introduction

Recently, bulk amorphous metals (BAM) or metallic glasses (BMG) have been attractive because of the higher interest in material science and engineering applications[1]. The Zr-based bulk amorphous metal exhibits an exceptional glass forming ability with a critical cooling rate of ~10 K/s and unique mechanical response, i.e. the abnormally high strength, bending ductility and fracture behavior[2,3]. Despite the remarkable properties of bulk amorphous metals, most BMGs fail by localized shear bands, which lead to catastrophic failure. It has been reported that the feature of fracture surface of amorphous metals under quasi-static loading could be characterized by the

* Corresponding author.

formation of shear bands and the vein pattern region which is contrast to the polycrystalline metallic materials.

The investigation of the high strain rate response of BMGs having superior intrinsic properties like high strength, low density and formation of shear bands are of importance issues in applications including ballistics and high-speed machining. Especially for the design of armor and anti-armor materials, the deformation and fracture behavior in bulk amorphous metals under impact condition should be also understood. However, available experimental data of dynamic mechanical properties under impact or shock loading for numerical simulation are limited[4~7]. According to recent results by using SHPB technique, the fracture strength of some BMG alloys showed a strain rate independent behavior up to 10^3 s^{-1}. In the design of kinetic penetrator, materials properties at the higher strain rate region exceeding 10^4 s^{-1} are necessary. Recently, the deformation behavior at high strain rate region was investigated by the author's group[8] that the strain rate dependence of the fracture strength in the Zr-based BMG appeared when the strain rate exceeded ~ 10^4 s^{-1}.

The purpose of this study is to investigate the influence of loading rate on the deformation and fracture behavior in the Zr-based bulk amorphous metal using an indentation method; over a wide strain rate range ($7x10^{-4}$ ~ about 10^5 s^{-1}) by the quasi-static and dynamic indentation tests using 3 mm WC balls and an explosive indentation test using a small detonator. For the controlled explosive indentation test, a small cylindrical detonator to give an extremely high strain rate to a small size target was adopted[9]. Also an interface-bonded specimen method, which facilitates the investigation of the formation of shear bands and deformation behaviors on the subsurface of the BMG sample, was tried.

2. Experimental Procedures

2.1. *Sample supplied*

Commercially available cast (Liquidmetal Technology) of 3.3 mm and 16 mm thick plates with the composition of $Zr_{41.2}Ti_{13.8}Cu_{12.5}Ni_{10}$ $Be_{22.5}$ were used. The chemical composition was determined using a JEOL SEM/EDX.

2.2. *Quasi-static and impact indentation test*

In order to investigate the deformation and damage behaviors in the Zr-based BMG, both quasi-static and dynamic indentation tests with a 3 mm diameter WC ball were performed to coupon shaped BMG specimen with a thickness of 3.3 mm. For quasi-static indentation testing, a hydro-servo machine (Instron 8516, Loadcell: 100 kN) was used.

On the other hand, a particle impact test with 3mm diameter WC balls was performed utilizing a laboratory built small scale air-gun in the velocity range of 30~250 m/s[10]. The impact surface of specimens was mirror polished to examine the occurrence of shear bands around the crater induced. The impact velocity of WC balls was measured to an accuracy of 3 % by timing their flight between two photo diodes situated close to the end of the gun barrel. After indentation tests, using the diameter of the crater formed on the specimen surface, the hardness and the mean strain induced under spherical indentation can be calculated[11].

2.3. *Controlled-explosive indentation test*

With a bonded-interface specimen sized 6x8x35 mm, a small explosive detonator with a diameter of 5 mm was glued on the interface area. Light vice pressure was applied to avoid the shattering of the specimen during impact. Figure 1 shows the experimental setup and geometry for the controlled explosive indentation by using an explosive detonator. The detonator was wrapped by stainless steel of 0.15 mm thickness and the stainless steel bottom disk with 5 mm diameter impacted on the surface of the BMG specimen, when it was detonated, which simulated the shock indentation of BMG materials. After indentation and detaching the specimen, the two separated sides of the specimen which represents subsurface damage morphology were cleaned and examined by the optical microscopy with interference contrast. SEM was used to observe the subsurface of damage zone with high magnification.

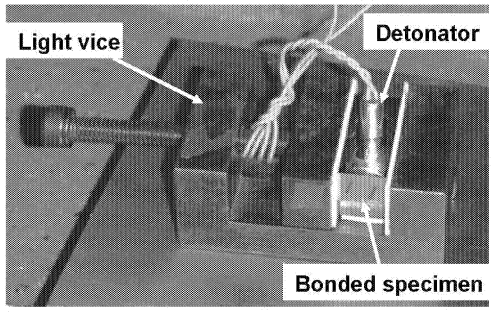

Fig. 1. Set-up for explosive indentation test using a small detonator of EBW to interface-bonded BMG specimen.

3. Experimental Results and Discussion

3.1. *Quasi-Static Indentation*

The quasi-static indentation of WC balls to Zr-based BMG produced the plastic deformation forming a crater at the indentation site. Figure 2 shows the relation between the crater diameter and the indentation load. At low indentation load, it produced only plastic deformation of the crater at the indentation site. As the indentation load increased, the crater diameter increased monotonically. When the indentation load exceeded 7 kN, it began to develop multiple shear bands around the crater. With further increasing of indentation load, shear bands became dense. Up to 20 kN, however, there was no spalling or chipping around the crater.

Under quasi-static indentation, the Zr-based BMG deformed as an elastic-plastic manner. It was a different behavior from that by the uniaxial compression test under plane stress state[8]. This might be due to the development of multiple shear bands under the constrained state as multi-axial stress state. Thus, it will be a promising trial to utilize the mechanism of multiple shear bands and the strain hardening behavior in order to improve the apparent ductility in BMGs.

The shear bands were developed both on the surface and on the subsurface of the interface bonded specimen formed by quasi-static indentation of WC ball and their

appearances are shown in Fig. 3. On the surface, multiple radial shear bands were developed at an angle of about 45 degree against the perimeter of the crater. At 20 kN,

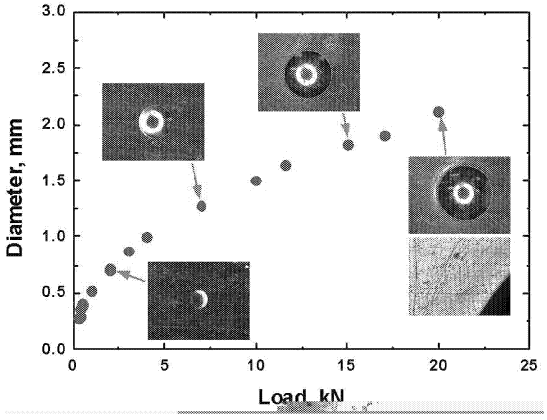

Fig. 2. Relation between crater diameter and indentation load obtained by quasi- static spherical indentation.

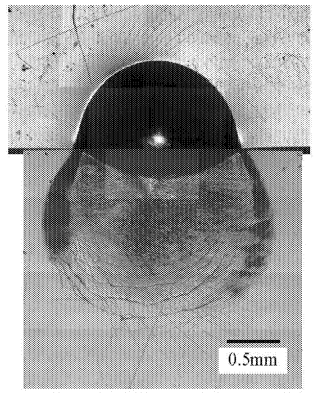

Fig. 3. Appearances of shear bands developed on surface and subsurface at the indentation load of 15 kN.

the pile up of deformation and the jog due to the consecutive development of circular shear bands were observed. The development of multiple shear bands was limited to the narrow region around the plastically deformed crater.

On the other hand, on the subsurface of the interface-bonded specimen, shear bands were developed densely in a circular shape underneath the crater. The radially developed ones initiated from the curved bottom of the crater crossing over each other and passed through the one along the circumferential direction, representing that the radial shear bands were developed later than the circumferential ones. The extension of multiple shear bands onto the subsurface underneath the crater corresponded to the size of plastically deformed region on the specimen surface. The density of shear bands developed decreased with depth. But the formation of cone cracks, which is common in the case of spherical indentation in brittle materials like glasses, was not observed on the subsurface.

3.2. *Dynamic Indentation*

The damage morphology at the surface after WC ball impact tests to Zr-based BMG were examined. In the case of the dynamic indentation of a WC ball to the Zr-based BMG sample, several different damage shapes could be observed depending upon the impact velocity of the WC ball. Figure 4 shows the variation of crater diameter and the change in damage morphology at the impact site with the impact velocity. It is a different behavior as compared with the quasi-static indentation cases previously shown in Fig. 2.

On the surface, at low impact velocity ranges, a crater was formed at the impact site. When the impact velocity exceeded 50 m/sec, edge chipping occurred instead of the shear bands formation around the crater. With increasing of impact velocity of WC balls, chipping became significant. Both edge spall and ring cracking within the craters occurred instead of the formation of multiple shear bands. Ring or partial ring cracks

often led to the extension of spall into the crater when the velocity was increased further to over 190 m/s. Therefore, when it exceeded 160 m/s, a rapid increase of crater diameter due to the occurrence of spalling can be seen in Fig. 4. Finally, in a higher impact velocity region over 200 m/s which corresponded to a high strain rate over $2x10^4$ s^{-1} [8], spall was extended to the entire area of the crater, which can be seen in Fig. 5. The SEM photograpy shows that the chipped part of the crater (designated as 1) was composed of vein-like pattern formed due to tensile stress and molten part. The plastically deformed part (designated as 2) indicates some evidence of melting on the surface. From these observations, it could be found that the overall spalling became dominant in the cases of dynamic indentation of WC balls to Zr-based BMG as the impact velocity increased, which is in contrast to the development of multiple shear bands in quasi-static indentation cases. Therefore, the formation of shear bands around the crater formed could be not observed. These variation in damage morphology in the case of dynamic indentation might have resulted because the contact duration during the spherical impact indentation was not enough to produce multiple shear bands around the crater on the surface. In the

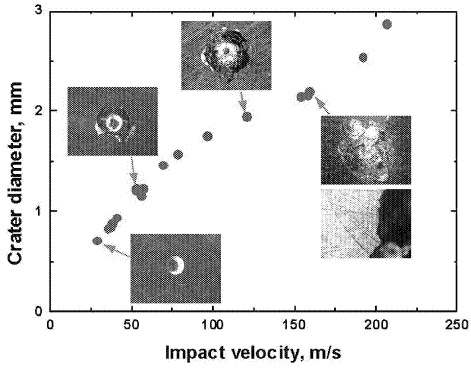

Fig. 4. Relation between crater diameter and impact velocity by dynamic indention.

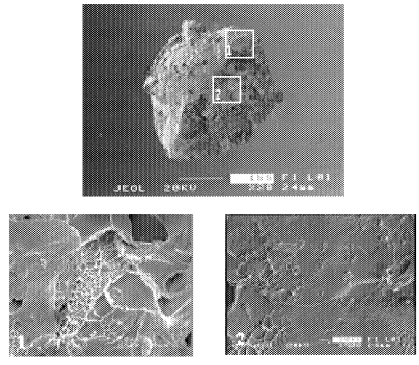

Fig. 5. SEM fractography of chipped crater caused by a WC ball impact at V=207 m/s.

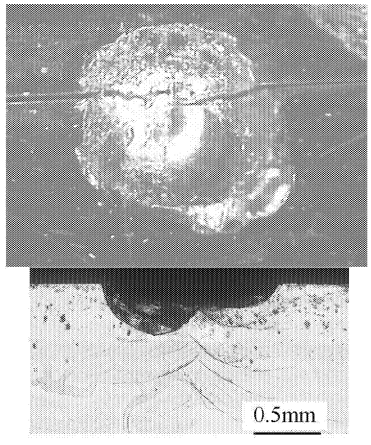

Fig. 6. A typical surface and subsurface damage morphology after a WC ball impact at V=106 m/s.

case of impact indentation representing a high strain rate over 10^4 s^{-1}, in addition, a rapid increase of temperature around the impact site produced local melting which caused chipping or spalling in the crater rather than the formation of multiple shear bands.

On the other hand, on the subsurface, only small numbers of radial shear bands were developed sparsely and crossing over each other, but no circumferential shear bands were observed. The radial shear bands did not develop fully. From these results, under dynamic indentation of WC balls to BMG specimen, the contact time is not enough to form multiple shear bands around the crater on the surface and subsurface. Therefore, the deformation and fracture behavior of bulk amorphous metals under dynamic loading condition was completely different from the case of quasi-static loading one.

3.3. *Explosive indentation*

Fig. 7 represents the surface and subsurface views in the interface-bonded BMG specimen which was explosively indented by using a small detonator. After the explosive indentation test, a crater corresponding to the diameter of the detonator and ring cracks around it were formed at the explosion site on the specimen surface. But the formation of shear bands around the crater was rarely observed, which is a similar behavior to the case of the WC ball impact indentation test. The explosive indentation did not last enough time to produce the shear bands around the crater because the loading duration was quite short. On the other hand, the subsurface damage was different from the former two cases and it can be classified into 3 regions; formation of adiabatic shear band representing a cone shape, significantly deformed region beneath the crater of a half-ellipse shape with a depth of 2.2~2.6 mm and slightly deformed region where an array of microcracks were developed in the interior region of the shear band crack. The cone cracks were linked to the ring crack developed on the surface. The significantly deformed region under the SEM examination showed the evidence of mechanical adhesion due to the melting at the interface during detonation indentation. Appearances of microcracks developed

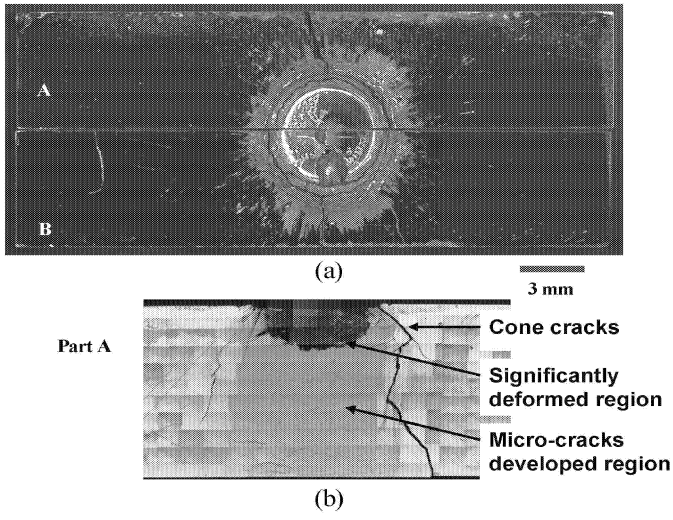

Fig. 7. Surface and subsurface views in the specimen explosively indented by small detonator.

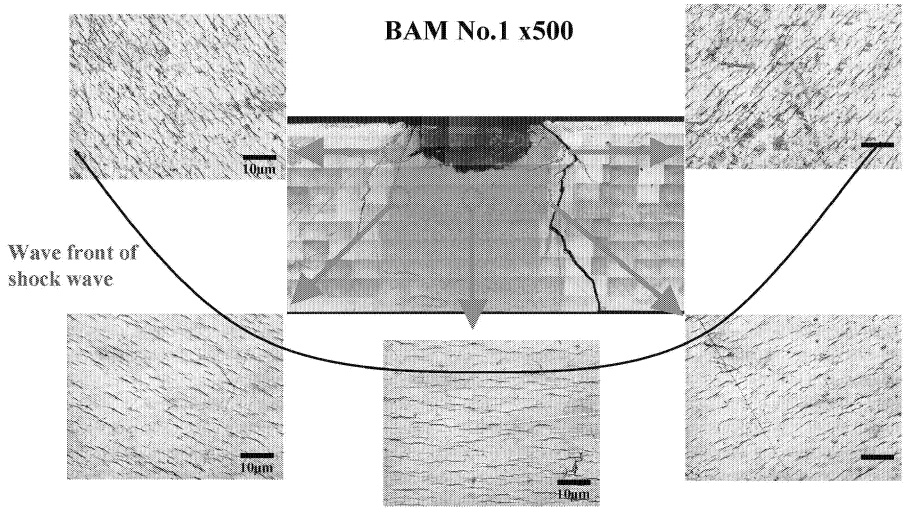

Fig. 8. Appearance of micro cracks developed underneath of the significantly deformed zone in Zr-BMG explosively indented by small detonator.

underneath of the significantly deformed zone in Zr-BMG by the explosive indentation were examined using microscope. As shown in Fig. 8, at the slightly deformed region, micro cracks were developed forming a circular shape along the wave front of shock wave within the interior region of the cone shaped shear band formed. With the increase of distance from explosion impact site, the microcracks formed were less dense and longer. The crack width range was changed from 3~7 μ m at the 3.9 mm depth to 6~15 μ m at the 9.1 mm depth. Under compressed and constraint conditions, microcracks were initiated along with shock wave front even under hypervelocity impact condition, but they did not connect to fully developed shear bands or cracks during the shock indentation

4. Conclusion

During quasi-static indentation tests of WC balls to Zr-BMG, multiple shear bands were developed around the plastically deformed crater when a static load reached to 7 kN. With increasing indentation load, shear bands became dense and well developed multiple shear bands were observed on the subsurface. In the case of dynamic indentation by 3 mm WC ball to Zr-BMG, variation of deformation occurred with increasing of the impact velocity; plastic deformation (crater), chipping (erosion). Shear bands were not observed around the crater, and instead chipping occurred. Few radially developed shear bands were observed on the subsurface of the impact site because the contact duration was not enough to form multiple shear bands around the crater both on the surface and the subsurface. In the case of explosive indentation to Zr-BMG, a crater of the same diameter as the detonator was formed on surface. The subsurface damage can be classified as cone shaped shear cracks, significantly deformed region and slightly deformed region

including microcracks formation. Under compressed and constraint conditions, short microcracks initiated along the shock wave front even under hypervelocity impact condition, but they could not develop due to short loading duration to connect to multiple shear bands.

Acknowledgments

This work was supported by Korean Research Foundation Grant funded by the Korean Government (MOEHRD) (KRF-2006-041-D00005).

References

1. H. A. Bruck, T. Christman, A. J. Rosakis and W. J. Johnson, *Scripta Metal. Mater.* **30**, 429 (1994).
2. P. Lowhaphandu, L. A. Ludrosky, S. L. Montgomery and J. J. Lewandowski, *Intermetallics* **8**, 487 (2000).
3. F. Szuecs, C. P. Kim and W. L. Johnson, *Acta Mater.* **49**, 1507 (2001).
4. T. Mukai, T. G. Nieh, Y. Kawamura, A. Inoue and K. Higashi, *Script. Mater.* **46,** 43 (2002).
5. H. A. Bruck, A. J. Rosakis and W. J. Johnson, *J. Mater. Res.* **11**, 503 (1996).
6. R. D. Conner, R. B. Dandliker, V. Scruggs and W. L. Johnson, *Int. J. Impact Eng.* **24**, 435 (2000).
7. G. Subhash, R. J. Dowding and L. J. Kecskes, *Mater. Sci. Eng.,* **A334**, 33 (2002).
8. H. S. Shin, D. K. Ko and S. Y. Oh, *J. Metastable Nanocrystal. Mater.,* **16-17**, 167 (2003).
9. D. K. Kim, J. H. Kim, Y. G. Kim, C. S. Lee, D. T. Chung, C. W. Kim, J. H. Choi and S. N. Chang, *Proc. Ceramic Armor and Armor System Symp.,* Nashiville, 93 (2003).
10. A. Wang, U. J. De Souza and H. J. Rack, *Wear* **151**, 157 (1991).
11. D. Tabor, *The Hardness of Metals* (Clarendon, Oxford, 1951).